Theor Appl Climatol (2010) 100:227–237
DOI 10.1007/s00704-009-0247-1

ORIGINAL PAPER

Statistical and dynamical characteristics of the urban heat island intensity in Seoul

Sang-Hyun Lee · Jong-Jin Baik

Received: 4 January 2009 / Accepted: 30 June 2009 / Published online: 19 January 2010
© Springer-Verlag 2010

Abstract The statistical and dynamical characteristics of the urban heat island (UHI) intensity in Seoul are investigated for non-precipitation days and precipitation days using 4-year surface meteorological data with 1-h time intervals. Furthermore, the quantitative influence of synoptic pressure pattern on the UHI intensity is examined using a synoptic condition clustering method. The statistical analysis shows that the daily maximum UHI intensity in Seoul for non-precipitation days is strongest in autumn (4.8°C) and weakest in summer (3.5°C). The daily maximum UHI intensity is observed around midnight in all seasons except in winter when the maximum occurrence frequency is found around 08 LST. This implies that anthropogenic heating contributes to the UHI in the cold season. The occurrence frequency of the UHI intensity has a negatively skewed distribution for non-precipitation days but a positively skewed distribution for precipitation days. The amplitude of the heating/cooling rate and the difference in the heating/cooling rate between the urban and rural areas are smaller in all seasons for precipitation days than for non-precipitation days, resulting in weaker UHI intensities for precipitation days. The urban cool island occurs very often in the daytime, with an occurrence frequency being 77% of the total non-precipitation days in spring. The analysis of the impact of large-scale dynamical forcing shows that the daily maximum UHI intensity varies with synoptic pressure pattern, ranging from −22% in spring to 28% in summer relative to the seasonal mean daily maximum UHI intensity. Comparison of the UHI intensity calculated using station-averaged temperatures to that based on the conventional two-station approach indicates that local effects on the UHI intensity are minimized by using multiple-station data. Accordingly, an estimation of the UHI intensity using station-averaged temperatures for both urban and rural areas is suggested.

S.-H. Lee · J.-J. Baik (✉)
School of Earth and Environmental Sciences,
Seoul National University,
Seoul 151-742, South Korea
e-mail: jjbaik@snu.ac.kr

1 Introduction

Understanding of the causes and effects of the urban heat island (UHI) has progressed based on observations in various cities (e.g., Oke 1973; Oke and Maxwell 1975; Eliasson 1996; Klysik and Fortuniak 1999; Chow and Roth 2006) and theoretical and numerical modeling (e.g., Vukovich et al. 1976; Baik et al. 2001; Atkinson 2003). These previous studies indicate that the UHI is not only influenced by urban physical and morphological features (e.g., roughness length, thermal inertia, canyon aspect ratio, and sky view factor) but also by meteorological conditions (e.g., wind speed, cloudiness, relative humidity, atmospheric stability, and thermal advection). Anthropogenic heat due to human activity also plays an important role in urban thermal and dynamical environments (Fan and Sailor 2005; Makar et al. 2006).

A key conclusion drawn from previous studies is that the UHI tends to develop more markedly in the nighttime under calm and clear weather conditions (Arnfield 2003). A large amount of incoming solar radiative energy can be absorbed at urban artificial surfaces during the daytime which can be compensated by nocturnal radiative cooling, consequently retarding the decrease of air temperature. On the other hand, in rural areas, nocturnal radiative cooling occurs more rapidly and a strong nocturnal inversion layer forms. The difference in surface energy balance between urban and

rural areas can explain the formation of a strong UHI under favorable weather conditions. Thus, wind speed and cloudiness, by which turbulent and radiative energy exchanges at ground surfaces are significantly changed, are considered as important meteorological factors that affect an UHI and are frequently used as predictors of the UHI intensity (e.g., Kim and Baik 2002).

Another key conclusion is that the strong UHI development is strongly associated with anticyclones. As expected, wind speed and cloudiness are subject to synoptic meteorological conditions. Relationships between synoptic weather types and the UHI are examined in many studies (e.g., Yague et al. 1991; Unger 1996; Morris and Simmonds 2000; Bejaran and Camilloni 2003). Morris and Simmonds (2000), for example, classified UHIs by intensity first and then determined synoptic conditions for each UHI intensity class using mean sea level pressure as a synoptic condition indicator. Another approach is to categorize synoptic weather types first and then analyze UHI characteristics in each class (Yague et al. 1991; Unger 1996; Bejaran and Camilloni 2003). These studies came to the same conclusions, even though the analysis methods were slightly different. The general characteristics and diversity of an UHI phenomenon are well documented by Oke (1982) and Arnfield (2003).

This study investigates the statistical and dynamical characteristics of the UHI intensity in Seoul, Korea first for both non-precipitation days and precipitation days. The characteristics of the UHI for precipitation days are not well examined in previous studies. Secondly, the impact of large-scale dynamical forcing on the daily maximum UHI intensity is examined using a synoptic condition clustering method. The influence of synoptic meteorological conditions on the UHI intensity in Seoul has never been examined yet. This study focuses on quantitative variations of the UHI intensity due to large-scale dynamical forcing rather than on the relationship between the UHI intensity and the synoptic weather type. Lastly, the issue regarding the determination of representative observation stations for the estimation of the UHI intensity in Seoul is discussed.

2 Description of the study region

Seoul is located in middle latitude and is classified as a temperate climate zone. It has an annual mean temperature of 12°C, an annual mean relative humidity of 67%, and an annual precipitation amount of 1,344 mm. The precipitation tends to concentrate in summer (from June to August), accounting for over half of the annual total precipitation amount. In addition, Seoul is one of the most densely populated cities in the world (Lee et al. 2009). The population of the city is about ten million. The total administrative area is 606 km^2, of which the urbanized area fraction (residential land, factory, school, road, etc.) is about 55%. Incheon is bordered on the east by Seoul and has a population of about 2.6 million. Gyeonggi province surrounds Seoul and is composed of wide areas of forest and agricultural land. The Yellow Sea is located west of the Korean peninsula. Diverse variations of the UHI are expected in Seoul because complicated interactions between synoptic winds and local circulations exist as well as geographical features are complex (Fig. 1).

3 Data and analysis methods

The UHI intensity is usually defined as an air temperature difference between an urban area and its surrounding rural

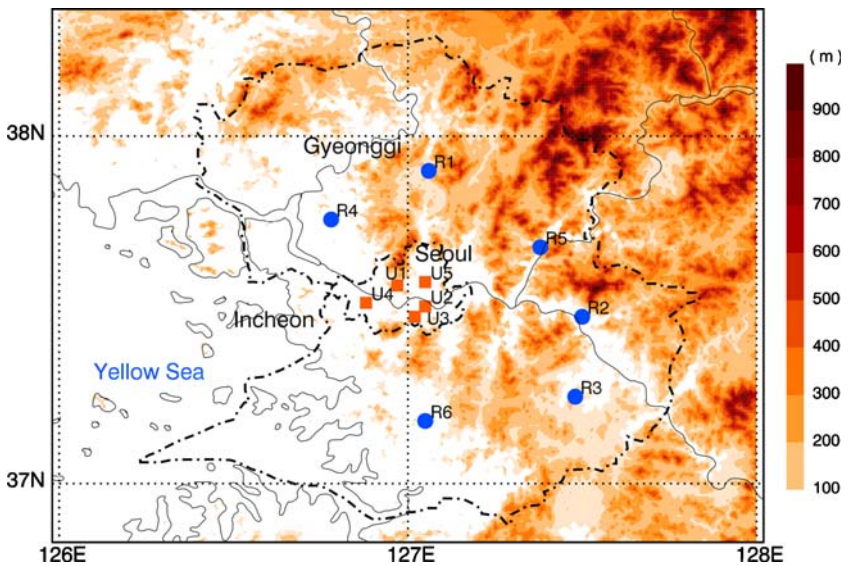

Fig. 1 Location of surface meteorological observation stations used to estimate the UHI intensity in Seoul. *Solid squares* and *circles* are representative stations for urban and rural areas, respectively. Local topography is shaded with a *vertical scale bar*. The administrative boundary is denoted by *dash-dot line*

area. In most previous studies, two representative urban and rural stations were used to calculate the UHI intensity (e.g., Jauregui 1997; Figuerola and Mazzeo 1998; Bejaran and Camilloni 2003; Kim and Baik 2004). Some studies used station-averaged temperature in both urban and rural areas (Gedzelman et al. 2003) or only in surrounding rural areas (Morris and Simmonds 2000; Morris et al. 2001) in order to better estimate the UHI intensity. The characteristics of the daily maximum UHI intensity in Seoul were investigated by Kim and Baik (2002) using data with 6-h time intervals at two representative stations.

In this study, the UHI intensity in Seoul is defined by station-averaged temperature for five representative urban stations minus station-averaged temperature for six representative rural stations (Fig. 1). The selected urban stations are located in highly urbanized areas in Seoul. The rural stations surround Seoul with a distance enough not to be affected by the urban area. The difference in mean elevation between the urban and rural stations is <5 m. Even though the influence of local circulations on each station is inevitable due to complex geographical features, the stations are selected in order to minimize local impacts on the UHI estimation. The analysis is conducted for a 4-year period from 1999 to 2002 on the basis of hourly observed data.

Synoptic pressure patterns are classified based on the synoptic pressure gradient over the area of interest to examine the quantitative variations of the UHI intensity due to large-scale dynamical forcing. The synoptic pressure gradient can be translated to dynamical meteorological forcing in the horizontal momentum equation. This forcing may affect local weather by modifying the intensity and duration of local circulations. The synoptic pressure disposition patterns are quantified using a geostrophic wind relation. This method differs from clustering methods of synoptic weather conditions (e.g., anticyclones, fronts) in previous studies. The classification applied here is implicitly related to local circulations and makes it possible to quantitatively investigate the impact of different synoptic dynamical forcing on the UHI intensity. Park and Yoon (1991) used this method to investigate the characteristics of local weather under various synoptic wind conditions over Korea for air quality applications.

The 850-hPa geopotential height fields of the National Centers for Environmental Prediction reanalysis data (Kalnay et al. 1996) are used to classify synoptic pressure patterns. The geostrophic wind speed and direction are estimated at a point (127.5° E, 37.5° N) using data at four surrounding points with the same longitudinal and latitudinal distances of 2.5°. Based on the calculated geostrophic wind components, wind directions are classified into four classes, northerly (315–45°), easterly (45–135°), southerly (135–225°), and westerly (225–315°), and wind speeds into two classes, weak (<5 m s^{-1}) and strong (≥5 m s^{-1}). The threshold wind speed of 5 m s^{-1} corresponds to a large-scale wind speed that possibly suppresses mesoscale circulation generated by horizontal inhomogeneity with a patch length of 20 km and an effective surface sensible heat flux of about 250 W m^{-2} (see Fig. 6 in Segal and Arritt 1992). Synoptic pressure patterns are therefore categorized into eight types in each season. Note that the estimated geostrophic wind components represent synoptic pressure disposition patterns over the Korean peninsula rather than actual wind speed and direction at the height.

The analysis is made separately for non-precipitation days and precipitation days in this study. A day having a total precipitation amount of over 5 mm is classified as a precipitation day, while a day with no precipitation is classified as a non-precipitation day (clear day). In addition, the day following one with a total precipitation amount of over 30 mm is excluded from non-precipitation days.

4 Analysis results

4.1 Features of the UHI

Figure 2 shows the spatial distribution of 2-m temperature over the Seoul metropolitan area at midnight in June and November 2002. These are drawn using temperatures observed at 47 stations. Typical concentric patterns are clear in both of these months, even though a warm region over the city is open toward the Yellow Sea in November due to the influence of relatively high sea surface temperature. The highest temperature region is located in Seoul, whereas the low temperature occurs in the north-eastern mountainous areas. A dual warm core, which is located in eastern and western parts within Seoul and is formed mainly due to land use inhomogeneity and local topography, is also found (Kim and Baik 2005).

Table 1 shows the seasonal mean daily maximum UHI intensity $\left(\Delta T_{\mathrm{u-r}}^{\max}\right)$ for non-precipitation days and precipitation days, along with 10-m wind speed and cloudiness. The daily maximum UHI intensity is strongest in autumn for both non-precipitation days and precipitation days and weakest in summer. Relatively high humidity and cloudiness, which are known to be negatively correlated with the UHI intensity (Arnfield 2003), are part of the cause of the low UHI intensity in summer. Actually, in summer, the Korean peninsula is mainly under the influence of the North Pacific High which is characterized by a warm and humid maritime air mass. The seasonal variation of the UHI intensity in Seoul (Table 1) is different from that in New York City, USA where the UHI intensities in summer and autumn (~4°C) are higher than those in spring and winter (~3°C; Gedzelman et al. 2003) and that in Wroclaw, Poland where the strongest UHI intensity is observed in spring and the weakest UHI intensity in autumn (Szymanowski 2005). The annual mean

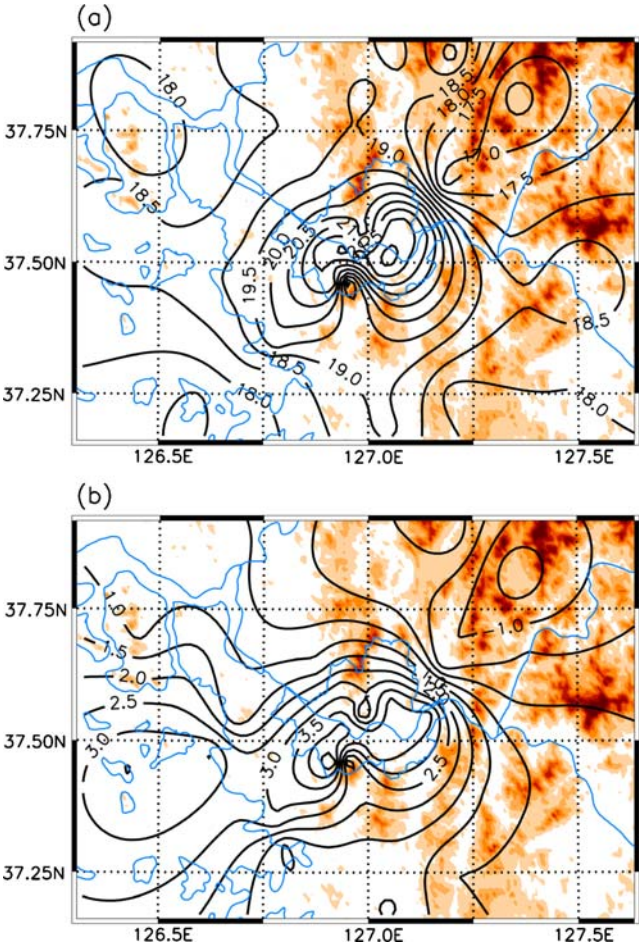

Fig. 2 Spatial distribution of monthly mean 2-m temperature at midnight in June (**a**) and November (**b**) 2002

daily maximum UHI intensity is 4.4°C for non-precipitation days and 2.6°C for precipitation days.

Figure 3 shows the frequency distribution of the daily maximum UHI intensity in each season as a function of UHI intensity for non-precipitation days. The total range of the daily maximum UHI intensity is very similar in all seasons with a range of 1–8°C. However, it is found that a stronger seasonal mean UHI intensity is related to a more negatively skewed distribution. The most negatively skewed distribution is observed in autumn. The difference in UHI intensity shown in Table 1 can be explained by the difference in the frequency distribution.

The difference in occurrence frequency distribution between non-precipitation days and precipitation days is very distinctive compared to that among seasons (Fig. 4). The daily maximum UHI intensity for non-precipitation days has a negatively skewed distribution with a maximum value of 27% at an interval of 4–5°C, while for precipitation days, it has a positively skewed distribution with a maximum value of 35% at an interval of 2–3°C.

The frequency distribution of the daily maximum UHI intensity for non-precipitation days is shown in Fig. 5 as a function of local time. Compared to the previous study of Seoul UHI intensity by Kim and Baik (2002), the exact occurrence time of the daily maximum UHI intensity is analyzed using 1-h time interval data. The maximum occurrence frequency is found around midnight (00 LST and 01 LST) in all seasons except for winter when the maximum occurrence frequency is found early in the morning (around 08 LST). The distinctive feature of the distribution in winter mornings can be partly explained by both anthropogenic heat emission in Seoul and the fact that a nocturnal atmospheric boundary layer in winter is relatively shallow. The estimated anthropogenic heat emission of Seoul in winter is over 35 W m^{-2} in the nighttime and reaches a peak value of about 70 W m^{-2} around 08–09 LST (Lee et al. 2009).

Figure 6 shows the frequency distribution of the daily maximum UHI intensity as a function of local time for both precipitation days and non-precipitation days. Similar to that for non-precipitation days (Fig. 5), a higher occurrence frequency of the daily maximum UHI intensity for precipitation days is found in the nighttime than in the daytime. However, there is a noticeable difference in occurrence time between precipitation days and non-precipitation days. The daily maximum UHI intensity is

Table 1 Seasonal statistics of the daily maximum UHI intensity and meteorological elements for non-precipitation days and precipitation days

	N	WS_u (m s^{-1})	WS_r (m s^{-1})	CL	ΔT_{u-r}^{max} (°C)
Non-precipitation days					
Spring	240	2.0 (0.6)	1.5 (0.5)	4.6 (3.0)	4.5 (1.3)
Summer	184	1.7 (0.5)	1.2 (0.4)	5.5 (2.7)	3.5 (1.0)
Autumn	235	1.4 (0.5)	1.0 (0.4)	4.7 (2.8)	4.8 (1.1)
Winter	154	1.8 (0.7)	1.2 (0.6)	3.9 (3.0)	4.5 (1.4)
Precipitation days					
Spring	29	2.0 (1.0)	1.5 (1.0)	6.1 (3.9)	2.6 (1.0)
Summer	78	1.7 (1.2)	1.0 (0.8)	7.6 (2.7)	2.4 (1.0)
Autumn	34	1.4 (0.8)	0.7 (0.6)	7.4 (3.7)	3.2 (1.4)
Winter	9	1.5 (1.0)	1.0 (0.6)	4.8 (4.8)	3.2 (1.6)

The value in parenthesis indicates the standard deviation. WS_u and WS_r denote mean wind speeds in the urban and rural areas, respectively. CL is cloudiness by a tenth. ΔT_{u-r}^{max} indicates the daily maximum UHI intensity. *N* is the number of occurrence day in each season

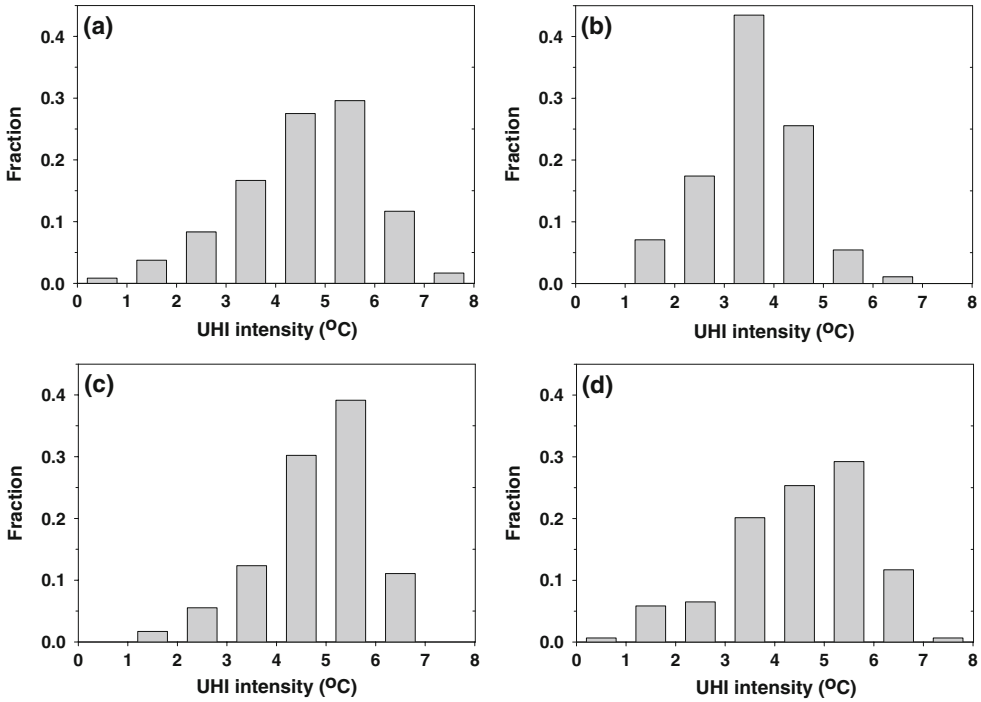

Fig. 3 Frequency distribution of the daily maximum UHI intensity as a function of UHI intensity in spring (**a**), summer (**b**), autumn (**c**), and winter (**d**) for non-precipitation days

observed before midnight (19–24 LST) for about 70% of precipitation days, while it is more likely to occur after midnight (24–08 LST) for non-precipitation days. This indicates that the daily maximum UHI intensity for non-precipitation days tends to appear at a later time after sunset compared to that for precipitation days.

Figure 7 shows the diurnal variation of the UHI intensity in each season for both non-precipitation days and precipitation days. The UHI intensity for non-precipitation days sharply increases in the evening and decreases in the morning in all seasons. The rapid increase/decrease of the UHI intensity is directly explained by the difference in heating/cooling rate between the urban and rural areas. The development of the UHI in winter lasts until sunrise with a high occurrence frequency, while it peaks around midnight and then gradually decreases in summer and autumn. The diurnal amplitude of the UHI intensity in summer is relatively small compared to other seasons partly due to high cloudiness and precipitation (Table 1). Under rainy weather conditions, stored heat at urban surfaces may be reduced due to lack of incoming shortwave radiation as well as evaporation of captured rain water at impermeable surfaces. Nocturnal radiative cooling is also limited by relatively high cloudiness and humidity. Furthermore, plenty of soil moisture in rural areas increases the rural thermal admittance, thereby reducing the difference in thermal admittance between urban and rural areas. As a consequence of these changes, the UHI intensity in precipitation days is weaker than that in non-precipitation days in all seasons (Fig. 7).

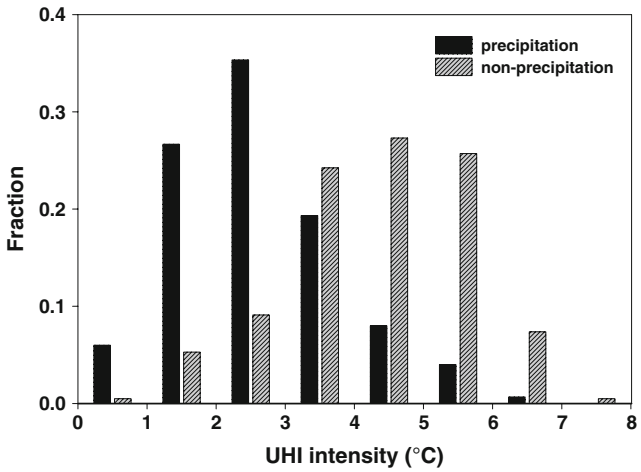

Fig. 4 Frequency distribution of the daily maximum UHI intensity as a function of UHI intensity for non-precipitation days and precipitation days

It is interesting to note that in the diurnal variation in spring, the UHI intensity has negative values for several hours during the daytime (Fig. 7a). The analysis shows that the occurrence frequency of the urban cool island (UCI) for non-precipitation days in Seoul is 77% (185 days) of the total non-precipitation days in spring, followed by 47% (73 days) in winter, 45% (83 days) in summer, and 29% (69 days) in autumn. A similar feature is also observed in New York City (Gedzelman et al. 2003).

For further interpretation of the diurnal variation of the UHI intensity, the seasonal mean heating/cooling rate in the urban and rural areas for non-precipitation days is shown in Fig. 8. The maximum heating rate is found during the 2–3 h after sunrise (around 09–10 LST) before a deep convective

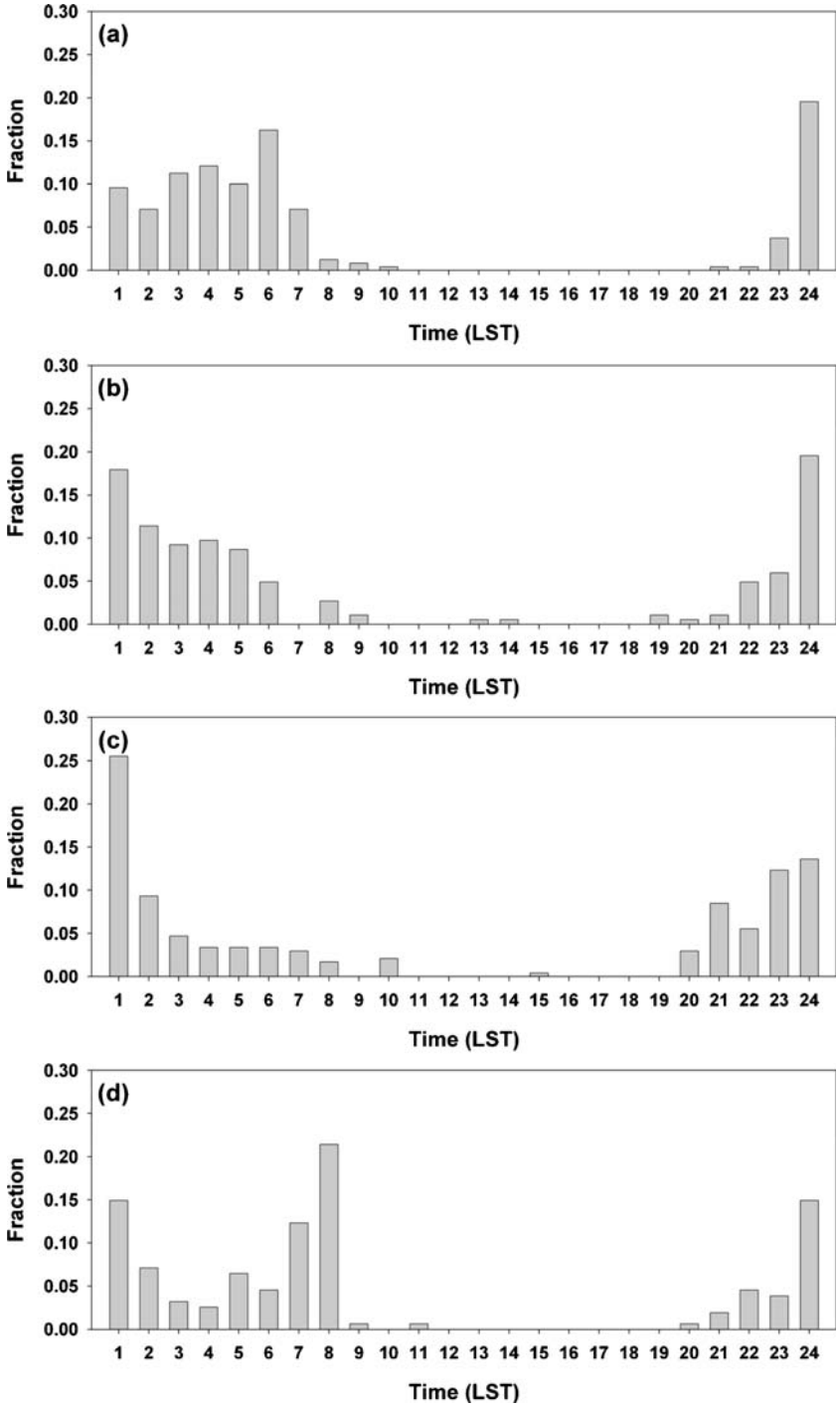

Fig. 5 Frequency distribution of the daily maximum UHI intensity as a function of local time in spring (**a**), summer (**b**), autumn (**c**), and winter (**d**) for non-precipitation days

boundary layer develops. The heating rate decreases gradually after this maximum, and the rate becomes negative around 15 LST when the air temperature is highest in the diurnal course. Even though these diurnal patterns are similar in both the urban and rural areas, the amplitude in the rural area is higher than that in the urban area in all seasons. The maximum heating rate in the rural area is about 2.5°C h^{-1} in all seasons except in summer when it has a maximum value of 1.6°C h^{-1}. The maximum cooling rate in the rural area is found in autumn with a value of −1.8°C h^{-1}. In the urban area, on the other hand, the maximum heating rate is about 1.5°C h^{-1}, while the maximum cooling rate is about −1.0°C h^{-1} in all seasons except in winter when the cooling rate is −0.5°C h^{-1} or less during the night. The summer maximum cooling rate is comparable to cooling rates observed in Montreal and Vancouver, Canada (Oke and Maxwell 1975). However, the nocturnal cooling rate in Seoul has a minimum value just

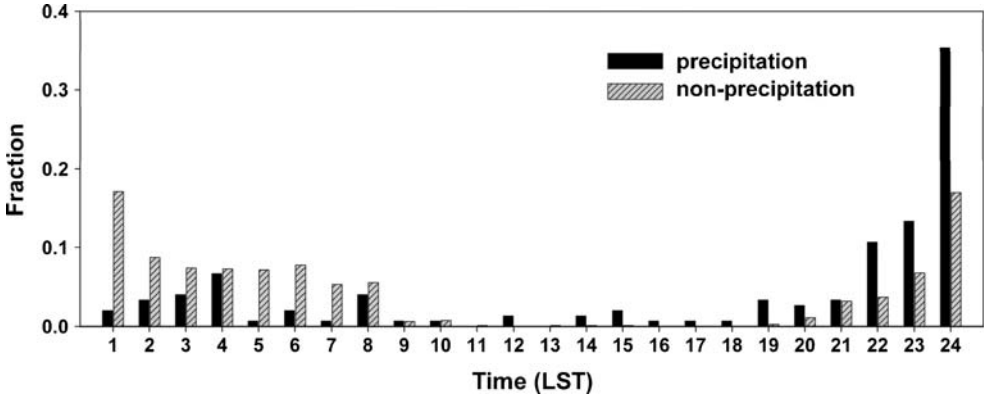

Fig. 6 Frequency distribution of the daily maximum UHI intensity as a function of local time for non-precipitation days and precipitation days

after sunset and converges into a value monotonically, whereas it fluctuates in those two cities.

Figure 9 shows the seasonal mean heating/cooling rate in the urban and rural areas for precipitation days. In general, there is a similarity between the results for non-precipitation days and precipitation days. However, for precipitation days, the amplitude of the heating/cooling rate and the difference in the heating/cooling rate between the urban and rural areas are reduced in all seasons, thereby resulting in weaker UHIs under rainy weather conditions. A reduction of maximum heating rates at both the urban and rural areas is prominent mainly due to lack of incoming solar radiation.

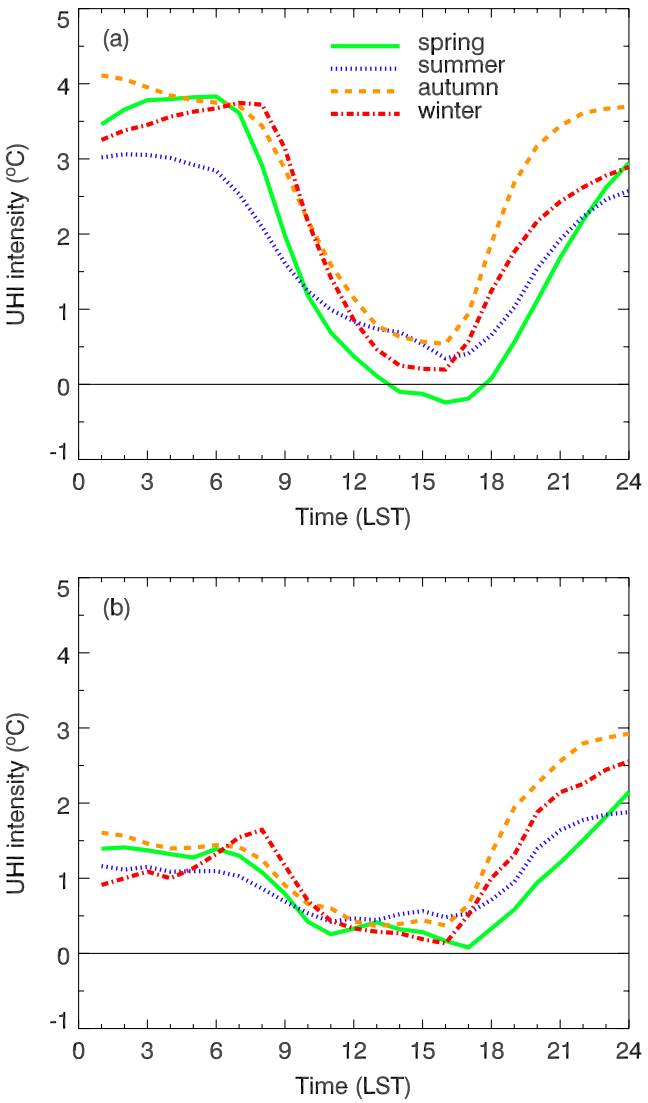

Fig. 7 Diurnal variation of the UHI intensity in each season for non-precipitation days (**a**) and precipitation days (**b**)

4.2 Variation in the UHI intensity under different synoptic pressure patterns

The variation of the daily maximum UHI intensity in Seoul under different synoptic pressure patterns is investigated using a synoptic condition clustering method. Table 2 shows synoptic classification results for non-precipitation days, along with the surface wind speed at the urban and rural stations, cloudiness, and the daily maximum UHI intensity. Westerly classes are predominant in all seasons because Korea is located in the westerly belt. The westerly classes take 75% of the total occurrence days in winter when Korea is under the influence of the Siberian High. On the other hand, the occurrence frequency of southerly classes is relatively high in summer when Korea is largely influenced by the North Pacific High. In general, the results in classification are similar to those of Park and Yoon (1991) in which 5-year data from December 1983 to November 1988 are analyzed. Furthermore, the mean surface wind speeds in both the urban and rural areas are linearly correlated with synoptic pressure gradients. This is a direct consequence of the dynamical clustering method used in this study. The mean cloudiness ranges from 0.9, for class N2 in winter, to 9.6, for class S2 in autumn. The daily maximum UHI intensity varies with synoptic pressure patterns by season. The highest UHI intensity is found for class W1 in autumn with a value of 5.2°C in which favorable weather conditions in surface wind speed and cloudiness are met. On the other hand, the lowest UHI intensity is found for class S2 in summer with a value of 3.0°C, which is mainly attributed to relatively high cloudiness.

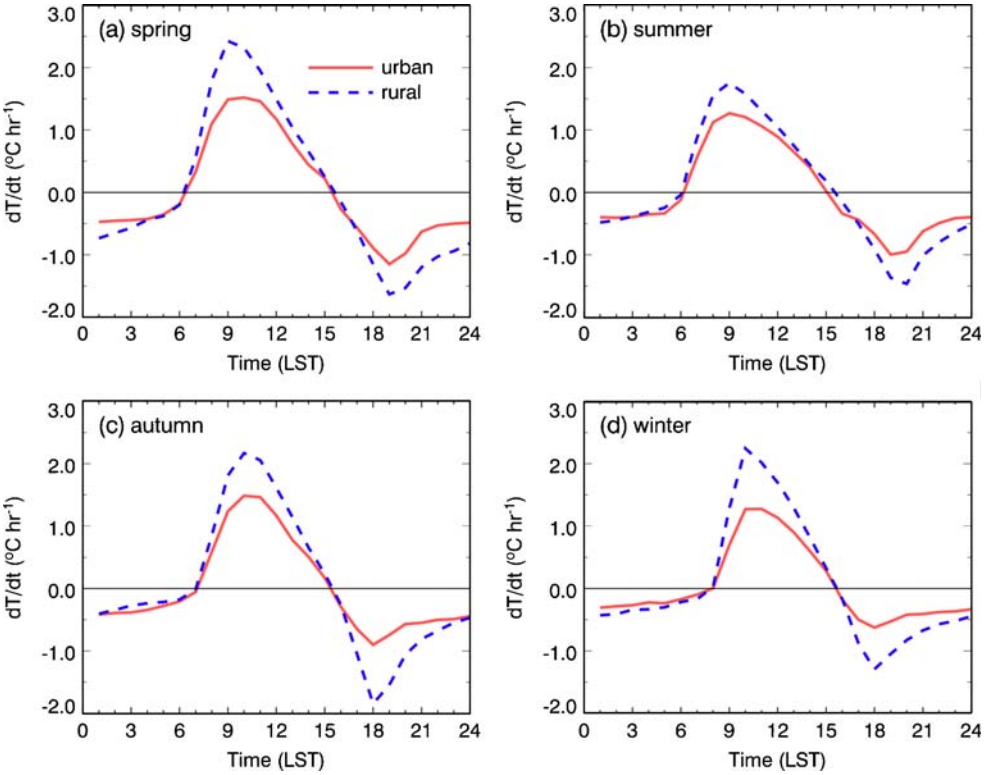

Fig. 8 Seasonal mean diurnal variation of the heating/cooling rate in the urban and rural areas for non-precipitation days. *Negative sign* means cooling rate

Figure 10 shows the fractional difference of the daily maximum UHI intensity of each synoptic pressure pattern for each season. The fractional difference is defined by $[(A-B)/B] \times 100\%$, where A is the daily maximum UHI intensity of each class and B is the seasonal mean daily maximum UHI intensity. The fractional difference is a measure of how much the daily maximum UHI intensity deviates from the seasonal mean daily maximum UHI

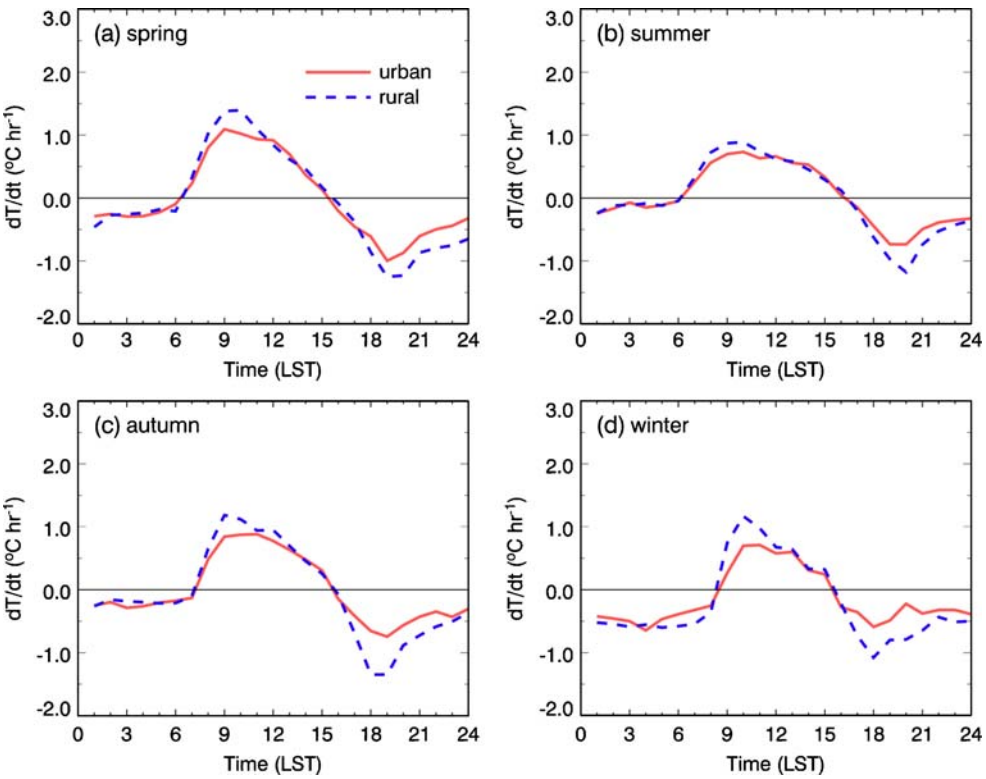

Fig. 9 Same as in Fig. 8 except for precipitation days

Table 2 Classification of synoptic pressure patterns for non-precipitation days during the four years of 1999–2002

	Class	*N* (%)	WS_g	WD_g	WS_u	WS_r	CL	ΔT_{u-r}^{max}
Spring	N1	12 (5)	3.0	353	1.8	1.4	4.6	4.5
	N2	31 (13)	6.9	340	2.2	1.6	3.2	4.4
	E1	6 (2)	2.9	90	1.4	1.2	4.7	4.6
	E2	4 (2)	9.8	119	2.1	1.6	9.2	3.6
	S1	11 (5)	3.2	185	1.5	1.2	6.4	4.7
	S2	12 (5)	7.6	192	1.7	1.4	7.2	4.5
	W1	30 (12)	3.2	268	1.6	1.2	5.2	4.6
	W2	134 (56)	8.6	278	2.1	1.6	4.3	4.6
Summer	N1	30 (16)	3.0	360	1.7	1.2	3.7	3.7
	N2	8 (4)	5.2	5	1.7	1.1	3.5	4.5
	E1	25 (14)	2.9	88	1.6	1.1	4.4	4.0
	E2	13 (7)	9.6	105	2.4	1.7	6.0	3.4
	S1	21 (11)	2.2	189	1.4	1.0	6.4	3.4
	S2	14 (8)	7.0	175	1.8	1.4	8.2	3.0
	W1	38 (21)	2.8	268	1.6	1.1	5.2	3.6
	W2	35 (19)	6.9	266	2.0	1.3	6.7	3.2
Autumn	N1	45 (19)	2.5	349	1.3	0.8	3.9	5.0
	N2	23 (10)	6.1	336	1.5	1.0	3.0	4.8
	E1	26 (11)	2.4	96	1.6	1.1	5.5	4.3
	E2	8 (3)	6.5	80	2.1	1.6	5.9	4.2
	S1	14 (6)	1.8	185	1.3	0.9	7.0	4.1
	S2	5 (2)	5.0	185	1.4	1.1	9.6	3.9
	W1	39 (17)	3.1	274	1.1	0.7	4.1	5.2
	W2	75 (32)	7.8	285	1.6	1.0	4.9	4.9
Winter	N1	8 (5)	3.0	346	1.8	1.1	5.3	3.8
	N2	24 (16)	11.3	326	2.2	1.6	0.9	3.6
	E1	3 (2)	4.2	67	1.4	1.3	5.7	4.0
	E2	0 (0)						
	S1	4 (3)	2.3	199	1.8	1.2	8.6	4.0
	S2	0 (0)						
	W1	14 (9)	2.9	280	1.4	0.9	5.5	4.4
	W2	101 (66)	9.7	293	1.8	1.2	4.0	4.8

Geostrophic wind speeds are divided into weak (<5 m s^{-1}) and strong (≥5 m s^{-1}) winds which are denoted by "1" and "2", respectively. Geostrophic wind directions are classified as northerly, easterly, southerly, and westerly winds which are marked with "N", "E", "S", and "W", respectively. WS_g and WD_g represent mean geostrophic wind speed and direction. *N* indicates the number of occurrence day for each class. The value in parenthesis represents the percentage of the occurrence in each season

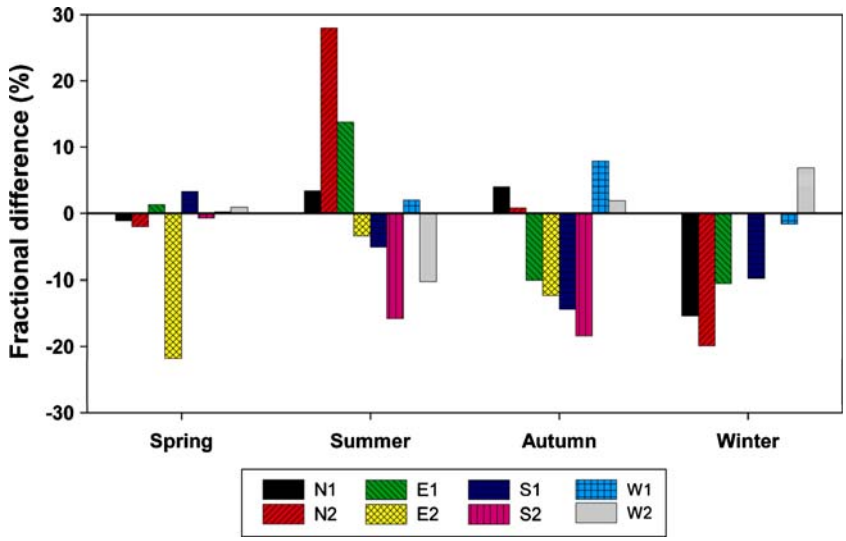

Fig. 10 Fractional difference of the daily maximum UHI intensity of each synoptic pressure pattern for each season

intensity due to different synoptic pressure patterns. The figure shows that the deviation of the daily maximum UHI intensity ranges from −22% in spring to 28% in summer relative to the seasonal mean UHI intensity. A large difference between class N2 and class S2 in summer is mainly caused by different synoptic conditions originating from continental and maritime air masses, respectively. The daily maximum UHI intensity is relatively weak in the classes of strong easterly and southerly geostrophic winds.

4.3 Representative observation stations for the Seoul UHI intensity

The UHI intensity is often quantified by the air temperature difference between urban and rural areas. It is therefore of primary importance to select representative observation stations for both the urban and rural areas. The estimated UHI intensity may vary with different urban/rural station comparisons. Here, UHI intensities in Seoul from two different urban/rural station sets are compared. One is calculated from the five urban stations and six rural stations adopted in this study (Fig. 1), and the other is calculated from an urban/rural station pair (U1 and R2 in Fig. 1). The latter two stations were used to estimate the UHI intensity in Seoul by Kim and Baik (2002). Station R2 is located eastern of Seoul (Fig. 1). Like most observation stations in the Seoul metropolitan area, station R2 can be easily influenced by local circulation due to its geographical location. In addition, the diurnal range of surface air temperature tends to increase with distance from the coast (Park and Yoon 1991).

Table 3 shows the seasonal mean daily maximum UHI intensity in Seoul calculated from the two urban/rural station sets for non-precipitation days in each season. The mean daily maximum UHI intensity by the station-averaged temperatures $\left(\Delta T_{\mathrm{u-r}}^{\max}\right)$ is stronger by up to 0.3°C than that by two observation stations $\left(\Delta T_{\mathrm{u-rW}}^{\max}\right)$ in spring and summer, whereas in autumn, $\Delta T_{\mathrm{u-rW}}^{\max}$ is larger than $\Delta T_{\mathrm{u-r}}^{\max}$ by 0.1°C. It is noticeable that when station-averaged temperatures are used to estimate the UHI intensity in Seoul, the standard deviation decreases in all seasons, especially in winter, when it decreases by 0.6°C. The more scattered feature of the UHI intensity in $\Delta T_{\mathrm{u-rW}}^{\max}$ is found in the results of different synoptic pressure patterns (not shown). These results indicate that even from a climatological perspective, it is a limitation in conducting a comparative study between cities as well as in estimating the UHI intensity quantitatively in a city using data from regular surface stations. Nevertheless, according to the analysis, the estimation of the UHI intensity using station-averaged temperatures is recommended in Seoul because it minimizes the local impact on the estimation of the UHI intensity to some extent.

Table 3 Seasonal mean daily maximum UHI intensity with standard deviation (in parenthesis) calculated from two different urban/rural station sets for non-precipitation days

	$\Delta T_{\mathrm{u-r}}^{\max}$	$\Delta T_{\mathrm{u-rW}}^{\max}$	$\mathrm{Pr_W}$
Spring	4.5 (1.3)	4.2 (1.7)	0.000
Summer	3.5 (1.0)	3.2 (1.2)	0.000
Autumn	4.8 (1.1)	4.9 (1.5)	0.004
Winter	4.5 (1.4)	4.5 (2.0)	0.855

$\Delta T_{\mathrm{u-r}}^{\max}$ and $\Delta T_{\mathrm{u-rW}}^{\max}$ indicate UHI intensities calculated by multiple stations and by two stations of U1 and R2, respectively. The significance value by statistical t test is represented in $\mathrm{Pr_W}$. The significance is a value in the interval [0,1], and a small value indicates that the two variables have significantly different means

5 Summary and conclusions

The statistical and dynamical characteristics of the UHI intensity in Seoul were investigated for non-precipitation days and precipitation days using the data of surface observation stations with 1-h time intervals during the period of 1999–2002. The statistical analysis showed that the seasonal mean UHI intensity is strongest in autumn and is weakest in summer. The occurrence frequency of the UHI intensity has a negatively skewed distribution for non-precipitation days but a positively skewed distribution for precipitation days. The daily maximum UHI intensity is observed more frequently around midnight for non-precipitation days, but in winter, the maximum occurrence frequency is found around 08 LST. This implies that the release of anthropogenic heat contributes to the UHI in the cold season. The daily maximum UHI intensity for non-precipitation days tends to appear at a later time after sunset compared to that for precipitation days.

The analysis of temporal characteristics showed that the maximum difference in the heating/cooling rate between the urban and rural areas occurs around sunrise and sunset. As a consequence, the UHI intensity rapidly increases in the evening and decreases in the morning in all seasons. The diurnal amplitude of the UHI intensity in summer is smaller than that in other seasons. The amplitude of the heating/cooling rate and the difference in the heating/cooling rate between the urban and rural areas are smaller in all seasons for precipitation days than for non-precipitation days, resulting in weaker UHI intensities for precipitation days. The UCI occurs very often during the daytime with a maximum occurrence frequency of 77% of total non-precipitation days in spring.

The analysis of the influence of synoptic pressure pattern on the UHI intensity showed that the difference in daily maximum UHI intensity due to different synoptic pressure patterns ranges from −22% in spring to 28% in summer

relative to the seasonal mean maximum UHI intensity. The highest daily maximum UHI intensity is found in class W1 of autumn with a value of 5.2°C, while the lowest UHI intensity is found in class S2 of summer with a value of 3.0°C.

The seasonal mean UHI intensity by station-averaged estimation was compared to that calculated using the data from two representative urban and rural stations. The result showed that in the case of station-averaged estimation, the standard deviation is reduced in all seasons, indicating that local impacts on the estimation of the UHI intensity are minimized by using multiple stations. Thus, the use of station-averaged temperatures is suggested in estimating the UHI intensity in Seoul.

It is worth noting that even though the influence of synoptic pressure patterns on the UHI intensity as well as the UHI difference between non-precipitation days and precipitation days is investigated, explicit explanations of the relevant physical processes that cause the resultant UHI might be limited only with observational data. An urban canopy model has a capability to represent various physical processes as well as physical and morphological properties in complex urban areas (e.g., Lee and Park 2008). In our future study, a mesoscale meteorological model coupled with an urban canopy model will be employed to examine physical mechanisms related to the observed UHI in Seoul and to assess the relative contributions of meteorological conditions and physical and morphological properties to the UHI.

Acknowledgments The authors are very grateful to two anonymous reviewers for providing valuable comments on this paper. This work was funded by the Korea Meteorological Administration Research and Development Program under Grant CATER 2006-2202.

References

Arnfield AJ (2003) Two decades of urban climate research: a review of turbulence, exchanges of energy and water, and the urban heat island. Int J Climatol 23:1–26

Atkinson BW (2003) Numerical modelling of urban heat-island intensity. Boundary-Layer Meteorol 109:285–310

Baik JJ, Kim YH, Chun HY (2001) Dry and moist convection forced by an urban heat island. J Appl Meteorol 40:1462–1475

Bejaran RA, Camilloni IA (2003) Objective method for classifying air masses: an application to the analysis of Buenos Aires' (Argentina) urban heat island intensity. Theor Appl Climatol 74:93–103

Chow WTL, Roth M (2006) Temporal dynamics of the urban heat island of Singapore. Int J Climatol 26:2243–2260

Eliasson I (1996) Urban nocturnal temperatures, street geometry and land use. Atmos Environ 30:379–392

Fan H, Sailor DJ (2005) Modeling the impacts of anthropogenic heating on the urban climate of Philadelphia: a comparison of implementations in two PBL schemes. Atmos Environ 39:73–84

Figuerola PI, Mazzeo NA (1998) Urban–rural temperature differences in Buenos Aires. Int J Climatol 18:1709–1723

Gedzelman SD, Austin S, Cermak R, Stefano N, Partridge S, Quesenberry S, Robinson DA (2003) Mesoscale aspects of the urban heat island around New York City. Theor Appl Climatol 74:29–42

Jauregui E (1997) Heat island development in Mexico City. Atmos Environ 31:3821–3831

Kalnay E, Kanamitsu M, Kistler R, Collins W, Deaven D, Gandin L, Iredell M, Saha S, White G, Woollen J, Zhu Y, Chelliah M, Ebisuzaki W, Higgins W, Janowiak J, Mo KC, Ropelewski C, Wang J, Leetmaa A, Reynolds R, Jenne R, Joseph D (1996) The NCEP/NCAR 40-year reanalysis project. Bull Am Meteorol Soc 77:437–471

Kim YH, Baik JJ (2002) Maximum urban heat island intensity in Seoul. J Appl Meteorol 41:651–659

Kim YH, Baik JJ (2004) Daily maximum urban heat island intensity in large cities of Korea. Theor Appl Climatol 79:151–164

Kim YH, Baik JJ (2005) Spatial and temporal structure of the urban heat island in Seoul. J Appl Meteorol 44:591–605

Klysik K, Fortuniak K (1999) Temporal and spatial characteristics of the urban heat island of Lodz, Poland. Atmos Environ 33:3885–3895

Lee SH, Park SU (2008) A vegetated urban canopy model for meteorological and environmental modelling. Boundary-Layer Meteorol 126:73–102

Lee SH, Song CK, Baik JJ, Park SU (2009) Estimation of anthropogenic heat emission in the Gyeong-In region of Korea. Theor Appl Climatol 96:291–303

Makar PA, Gravel S, Chirkov V, Strawbridge KB, Froude F, Arnold J, Brook J (2006) Heat flux, urban properties, and regional weather. Atmos Environ 40:2750–2766

Morris CJG, Simmonds I (2000) Associations between varying magnitudes of the urban heat island and the synoptic climatology in Melbourne, Australia. Int J Climatol 20:1931–1954

Morris CJG, Simmonds I, Plummer N (2001) Quantification of the influences of wind and cloud on the nocturnal urban heat island of a large city. J Appl Meteorol 40:169–182

Oke TR (1973) City size and the urban heat island. Atmos Environ 7:769–779

Oke TR (1982) The energetic basis of the urban heat island. Q J R Meteorol Soc 108:1–24

Oke TR, Maxwell BB (1975) Urban heat island dynamics in Montreal and Vancouver. Atmos Environ 9:191–200

Park SU, Yoon IH (1991) The characteristic features of local weather phenomena under the various synoptic winds over South Korea. J Korean Meteorol Soc 27:87–118

Segal M, Arritt RW (1992) Nonclassical mesoscale circulations caused by surface sensible heat-flux gradients. Bull Am Meteorol Soc 73:1593–1604

Szymanowski M (2005) Interactions between thermal advection in frontal zones and the urban heat island of Wroclaw, Poland. Theor Appl Climatol 82:207–224

Unger J (1996) Heat island intensity with different meteorological conditions in a medium-sized town: Szeged, Hungary. Theor Appl Climatol 54:147–151

Vukovich FM, Dunn J, Crissman B (1976) A theoretical study of the St. Louis heat island: the wind and temperature distribution. J Appl Meteorol 15:417–440

Yague C, Zurita E, Martinez A (1991) Statistical analysis of the Madrid urban heat island. Atmos Environ 25B:327–332